

Microphysical characteristics of precipitation within convective overshooting over East China observed by GPM DPR and ERA5

Nan Sun¹, Gaopeng Lu¹, Yunfei Fu¹

¹School of Earth and Space Sciences, University of Science and Technology of China, Hefei, 230026, China

Corresponding to: Yunfei Fu, fyf@ustc.edu.cn

Abstract. We examine ~~the~~ geographical distribution ~~and pattern of convective overshooting and its internal~~ microphysical three-dimensional structure of ~~convective overshooting~~precipitation over East China by matching Global Precipitation Measurement Dual-frequency Precipitation Radar instrument (GPM DPR) with European Centre for Medium-Range Weather Forecasts 5th Reanalysis (ERA5). Convective overshooting~~events~~ mainly occur over ~~Northeast China, NC~~(~~NC~~Northeast China) and northern ~~Middle and East China, MEC~~(~~MEC~~Middle and East China) ~~and its frequency varies from~~ 4×10^{-4} to 5.4×10^{-3} , ~~with a magnitude of only 10^{-3} .~~ Radar reflectivity of convective overshooting over NC accounts for a higher proportion below the ~~zero-freezing~~ level, while MEC and ~~South China, SC~~(~~SC~~South China) account for a higher proportion above the ~~zero-freezing~~ level, indicating stronger upward motion and more ice crystal particles; ~~—~~ The microphysical processes within convective overshooting are unique, leading to various properties of the droplets in precipitation. ~~Droplets of convective overshooting are large, but sparse. And its effective radius of droplet, below 10 km altitude, is almost exceeding 2.5 mm, which is about twice than normal precipitation. Convective overshooting humidifies air below the cloud top and obviously increases the ozone near tropopause as a result of influx of ozone from lower troposphere and sinking of air with high concentration ozone in the stratosphere.~~ Findings of this study may have important implications for the microphysical evolution associated with convective overshooting, and provide more accurate precipitation microphysical parameters ~~as input for model simulations, as the input of the model simulation.~~

带格式的：上标

带格式的：上标

带格式的：字体：10 磅

29

30 1 Introduction

31 Convective overshooting provides a rapid transport mechanism that can irreversibly transport water
32 vapor and chemical constituents from lower troposphere to the upper troposphere and lower stratosphere
33 (UTLS) by mixing them with environmental air (Fueglistaler et al., 2004; Frey et al., 2015), which has a
34 direct impact on radiation balance and global climate change (Solomon et al., 2010). As one of the main
35 sources of ozone destroying OH hydroxyl radicals, stratospheric water vapor can help to destroy ozone,
36 which has potential effects on radiative forcing (Anderson et al., 2012). Water vapor enters the
37 stratosphere mainly through the tropical tropopause layer. Previous Several studies show that tropical
38 convective overshooting has a net dehydrating effect on the stratospheric humidity (Danielsen, 1993;
39 Sherwood and Dessler, 2001 ~~), while Recently, modeling and observational studies have universally~~
40 show ~~the tropical moistening effect of~~ convective overshooting ~~hydrating on~~ the stratosphere
41 (Chaboureau et al. 2007; Jensen et al. 2007; de Reus et al. 2009; Avery et al. 2017) because of the
42 injection of ice mass into the stratosphere (Grosvenor et al., 2007; Corti et al., 2008; Chemel et al., 2009;
43 Khaykin et al., 2009). ~~In addition to these impacts on water vapor, the convective overshooting affecting~~
44 ~~on the UTLS temperature has also attracted much attention (Sherwood et al., 2003; Chae et al., 2011;~~
45 ~~Biondi et al., 2012).~~In midlatitude, observations and model simulations show that deep convective
46 overshooting is also an important source for the lower stratospheric water vapor (Liu and Liu, 2016;
47 Smith et al., 2017; Liu et al., 2020; Werner et al., 2020; Wang et al., 2023). Wang et al. (2023) use a
48 high-resolution numerical model to study convective overshooting moistening in the midlatitude lower
49 stratosphere and results show that convective water vapor plumes above 380-K temperature are stable
50 in the stratosphere, while that closer to the tropopause and cloud tops are less stable. In addition to these
51 impacts on water vapor, the effects of convective overshooting on the temperature of the UTLS have also
52 attracted much attention (Sherwood et al., 2003; Chae et al., 2011; Biondi et al., 2012).

53 In addition to UTLS composition effects, convective overshooting is often associated with severe and
54 hazardous weather (e.g., heavy rain, hail, tornadoes, and strong winds) at the Earth's surface, with
55 important social and economic impacts ~~on society and economy~~ (Line et al., 2016; Bedka et al., 2018;
56 Marion et al., 2019). Given these potentially significant impacts, it's is of high importance to understand

带格式的：字体：(中文)+中文正文(宋体)，(中文)中文(中国)

57 | the characteristics of convective overshooting, which have attracted considerable attention in recent
58 | years (Johnston et al., 2018; Muhsin et al., 2018).

59 | Perhaps one of the most poorly understood features of convective overshooting is the microphysical
60 | structure of precipitation, such as particle size, concentration, phase state and other parameters.
61 | Understanding the microphysical characteristics of convective overshooting is helpful to clarify the
62 | efficiency of water vapor transported to the lower stratosphere by convective overshooting. In addition,
63 | the microphysical processes within convective overshooting are closely related to storm dynamics and
64 | thermodynamics through latent heat, and the quantitative description of microphysical characteristics is
65 | helpful to improve the accuracy of model simulation parameters (Homeyer and Kumjian, 2015). Liu et al.
66 | (2012) studied the climatological characteristics of convective overshooting and found convective
67 | overshooting show remarkable regionality and seasonal variations, that rain rates of convective
68 | overshooting are bigger than that of deep convection. Homeyer and Kumjian (2015) observed the radar
69 | reflectivity characteristics ~~within of the~~ convective overshooting from the analysis of the polarimetric
70 | radar observations. Although the above studies have explored the characteristics of some precipitation
71 | parameters within convective overshooting, we still lack the understanding of more precipitation
72 | microphysical parameters and more detailed microphysical processes within convective overshooting
73 | due to the limitations of observation methods.

74 | To fully study the microphysical characteristics of convective overshooting, accurate methods of
75 | detecting the frequency and long-term distribution of convective overshooting are required. The
76 | traditional way for detecting convective overshooting from satellite is to find pixels in infrared
77 | imagery ~~ways for detecting convective overshooting is to find pixels~~ with brightness temperatures colder
78 | than a given temperature threshold (Machado et al. 1998; Rossow and Pearl 2007). Gettelman et al.
79 | (2002) have studied the cloud regions colder than the tropopause temperature on infrared images and
80 | found that the frequency of tropical convective overshooting is about 0.5%. However, it is impossible to
81 | guarantee that the low value of infrared brightness temperature represents clouds penetrating the
82 | tropopause rather than cirrus or cloud anvil in the upper air due to the lack of vertical structure
83 | information of convection. Also, overshoots mix with relatively warm stratosphere air such that cold
84 | pixels are often diminish and not a reliable means to identify overshooting. With the launch of
85 | Precipitation Radar aboard Tropical Rainfall Measuring Mission (TRMM), three-dimensional structure
86 | information of precipitation within the convective overshooting can be provided (Alcala and Dessler,

87 2002; Liu and Zipser, 2005) and a new method for detecting the convective overshooting is proposed that
88 is to ~~fine-find~~ pixels with rain top height higher than tropopause height (Xian and Fu, 2015; Sun et al.,
89 2021), which improves the accuracy of detecting convective overshooting. Still, TRMM PR can't
90 provide the precipitation microphysical information, which limits our study on the internal
91 microphysical structure within convective overshooting. Besides, TRMM PR can underestimate the
92 height of convective overshooting because of only sensitive to large precipitation particles (sensitivity at
93 ~17 dBZ) (Hanii and Zheng, 2014).

94 As the continuation of TRMM PR, Global Precipitation Measurement (GPM) carrying the first
95 Dual-frequency Precipitation Radar (DPR) launched in February 2014. GPM DPR include two bands of
96 precipitation radar, which provides excellent opportunities for studying the microphysical structure of
97 precipitation (Sun et al., 2022a). Liu et al. (2016, ~~2019~~2020) have used GPM KuPR and ERA-Interim
98 6-hourly ~~dataset~~data set to study climatology and detection of convective overshooting. However, the
99 above studies only use the KuPR data and mainly focus on the geographical distribution, ~~the~~
100 microphysical processes of convective overshooting remain unknown. ~~Besides, the matching time~~
101 ~~between GPM and ERA-Interim is too long (6 hour) to ensure the accuracy of convective overshooting~~
102 ~~detection.~~

带格式的: 字体: (中文) +中文正文 (宋体), (中文) 中文(中国)

103 Another difficulty in convective overshooting detection is to obtain tropopause height data with high
104 spatial and temporal resolution. On the one hand, the determination of the tropopause is still under debate.
105 At present, the following ~~two~~four definitions of the tropopause are widely adopted throughout the world:
106 ~~one is the eCold point~~ tropopause, ~~and the other is the thermodynamic thermal~~ dynamic
107 ~~tropopause and ozone tropopause.~~ However, the eCold point tropopause is only physically meaningful in
108 the latitude zone 10°S-10°N near the equator (Highwood and Hoskins, 1998; Rodriguez-Franco and
109 Cuevas, 2013). ~~Dynamic tropopause is based on the differing values of potential vorticity in the~~
110 ~~troposphere and stratosphere, which applies to extratropical areas (Danielsen et al., 1987; Holton et al.,~~
111 ~~1995). Ozone tropopause is defined based on the ozone sounding profiles, whose disadvantage is that~~
112 ~~the choice of ozone mixing ratio thresholds varies with region and season (Bethan et al., 1996; Zahn et~~
113 ~~al., 2004).~~ Therefore, this paper uses the ~~thermodynamic thermal~~ tropopause, which is defined by the
114 World Meteorological Organization (WMO) (WMO, 1957). The ~~thermodynamic thermal~~ tropopause is
115 based on the temperature lapse rate, also known as lapse-rate tropopause. The accurate calculation of the
116 tropopause height based on this definition, on the other hand, depends on the temperature profile data

117 with high spatial and temporal resolution. The latest generation of reanalysis data ERA5 provides hourly
118 estimates of a large number of atmospheric, land and oceanic climate variables, which has attracted much
119 attention due to its much higher spatial and temporal resolution than its predecessor ERA-Interim,
120 especially in the upper troposphere and lower stratosphere (Hoffmann et al. 2019). Sun et al. (2022b)
121 verified the accuracy for the tropopause height calculated from temperature profiles of ERA5 by
122 comparing ERA5 with other popular datasets.

123 East China is located in the East Asian monsoon region, with unique climate characteristics. The
124 precipitation of East China in summer is affected by the circulation anomalies of the East Asian tropical
125 and subtropical monsoon and their interactions. The precipitation anomalies not only have an important
126 impact on industrial and agricultural production, social infrastructure construction, but also threaten the
127 safety of human life and property. Many scholars have studied the characteristics of precipitation in East
128 China (Zhang et al., 2018; Xu, 2020), but few have studied the characteristics of convective overshooting
129 and its internal precipitation microphysical structure over East China. The purpose of this study is to
130 examine the microphysical characteristics of convective overshooting over East China by matching the
131 precipitation data from GPM DPR and meteorological parameters from ERA5.

132 **2 Data and method**

133 **2.1 DPR-based precipitation dataset**

134 GPM DPR include KuPR (Ku band, 13.6 GHz) and KaPR (Ka band, 35.5 GHz), two bands of
135 precipitation radar. KuPR is similar to TRMM PR and has a longer wavelength, which is better at
136 detecting heavy precipitation (the minimum detected precipitation is about 0.5 mm/h). However, KaPR
137 has a shorter wavelength, which is more sensitive to weak precipitation (the minimum detected
138 precipitation is about 0.2 mm/h). Based on the different echo characteristics of Ku band and Ka band, the
139 dual channel inversion algorithm can be used to retrieve Droplet Size Distribution DSD (~~DSD~~Droplet
140 Size Distribution). Here we use the precipitation datasets are provided by the GPM level 2 product
141 2ADPR in version 6 ~~from 2014 to 2020 in summer (June, July and August)~~. The horizontal resolution is
142 5 km and the vertical resolution is 125m. The precipitation microphysical parameters provided by GPM
143 2ADPR include droplet concentration (dBN_0) and effective radius (D_0).

144 **2.2 ERA5-based meteorological dataset**

145 The meteorological data are from ERA5 reanalysis product, whose name is “ERA5 hourly data on
146 pressure levels from 1940 to present”. datasets. And the following parameters are used in this paper:
147 temperature, specific humidity, vertical velocity, ozone mass mixing ratio, U-component of wind, and
148 V-component of wind. The time resolution is 1 h and the horizontal resolution is $0.25^\circ \times 0.25^\circ$. Vertical
149 coverage is 1000 hPa to 1hPa and vertical resolution is 37 pressure levels (1000, 975, 950, 925, 900,
150 875, 850, 825, 800, 775, 750, 700, 650, 600, 550, 500, 450, 400, 350, 300, 250, 225, 200, 175, 150, 125,
151 100, 70, 50, 30, 20, 10, 7, 5, 3, 2, 1 hPa).

带格式的: 字体: (中文) +中文正文 (宋体), (中文) 中文(中国)

152 **2.3 ~~Definition~~ Detection method of the convective overshooting**

153 ~~The convective overshooting is defined as the storm top height above the real time tropopause height.~~
154 ~~storm top height is obtained from the GPM DPR. Tropopause height is calculated from the temperature~~
155 ~~profiles from ERA5 according to the definition from the World Meteorological Organization, whose~~
156 ~~characteristics are as follow: (1) the atmospheric lapse rate is 2 K km^{-1} or less and (2) the atmospheric~~
157 ~~lapse rate does not exceed 2 K km^{-1} between the tropopause level and all higher levels within 2 km~~
158 ~~(WMO, 1957).~~

带格式的: 上标

带格式的: 上标

159 Firstly, match each pixel of GPM DPR detection with ERA5 grid data by using the principle of the
160 nearest method. The marching time between GPM and ERA5 is 1 h, and the matching range is $0.25^\circ \times$
161 0.25° . Storm top height is obtained from the GPM DPR. Convective overshooting is defined to occur
162 where the storm top height is above the real-time tropopause height in a precipitation pixel.

163 Real-time tropopause height is calculated from the temperature profiles from ERA5 according to the
164 definition from the World Meteorological Organization (WMO, 1957). The algorithmic process is
165 shown as follows: Firstly, find X layer whose atmospheric lapse rate is 2 K km^{-1} or less starting from
166 the first layer (near the ground) of the temperature profile, and then judge whether the atmospheric
167 lapse rate does not exceed 2 K km^{-1} between the X level and all higher levels within 2 km, if so, the
168 height of X layer is the tropopause height, if not, repeat the above algorithm starting from the X layer
169 until tropopause layer is found.

带格式的: 上标

带格式的: 上标

带格式的: 字体: (中文) +中文正文 (宋体), (中文) 中文(中国), (其他) 英语(美国)

170 **2.4 Study areas**

171 The study areas are marked as black boxes in Fig. 1a and only the land parts are studied because
172 characteristics of vertical structure of precipitation over land and sea are very different, and this study
173 is limited in space and focuses only on the land region. To have a better understanding of precipitation
174 microphysical structure over different regions of East China, we divided the study areas into three parts
175 according to its climatic characteristics and previous studies (Sun et al., 2022a). Using years of
176 NCEP/NCAR reanalysis data, Xia (2015) analyzed the climatic feature of temperature and water vapor
177 in China and divided China into different climatic zones. To have a better understanding of precipitation
178 microphysical structure over different regions of East China, we also divided East China into three
179 climatic zones according to its climatic characteristics and previous studies (Xia, 2015; Sun et al., 2022a).
180 From north to south, they are Northeast China NC (NC Northeast China, 38 °-50 °N, 118 °-130 °E),
181 Middle and East China MEC (MEC Middle and East China, 26.5 °-38 °N, 112 °-123 °E), and South China
182 SC (SC South China, 18 °-26.5 °N, 108 °-123 °E). For the three regions, the lower latitude areas have
183 higher surface temperature, greater temperature lapse rate and lower temperature of stratosphere.
184 Temperature profiles of same latitude are essentially same over SC and MEC, and temperature signals
185 exist meridional differences over NC. Atmospheric humidity has remarkable regional characteristics.
186 SC is wetter, with the surface relative humidity of more than 70%, while NC and MEC are drier and
187 their humidity range from 50% to 70% (Xia, 2015). The study time frame is defined as the time from
188 2014 to 2020 in summer (June, July and August).

带格式的: 字体: (中文) +中文正文 (宋体), (中文) 中文(中国)

189 **3 Results**

190 **3.1 Case studies**

191 Three cases selected from NC, MEC and SC are analyzed to lay a foundation for the subsequent
192 statistical analysis. The precipitation characteristics of the three cases are shown as Fig. 2. The Case 1
193 (C1) occurs in NC at 14:00 on July 1, 2017. Convective overshooting is observed in a A total of 65 pixels
194 for C1, in which convective overshooting occurs and their whose mean rain rate are mostly over 20.7
195 mm/h (Fig. 2a) and their-mean storm top height are over 14.142 km (Fig. 2b). The strong radar
196 reflectivity along A1B1 occurs at 35-95km away from point A1, and the strongest echo is up to 50 dBZ,
197 appears at 0-5 km (Fig. 2c). The maximum echo height is about 15 km, 2 km higher than the tropopause

带格式的: 字体: (中文) Times New Roman

带格式的: 字体: (中文) Times New Roman

198 height. The Case 2 (C2) occurs in MEC at 13:00 on July 30, 2015. Convective overshooting is observed
199 in a total of 58 pixels for C2. in which convective overshooting occurs and their mean rain
200 rate are more than 29.725 mm/h (Fig. 2d) and their mean storm top height are mostly over 15.214 km
201 (Fig. 2e). The radar echo along A2B2 is very strong and the strongest echo is up to 50 dBZ, which is
202 about 45-95 km away from point A2 (Fig. 2f). The highest echo can reach to about 17 km altitude. The
203 Case 3 (C3) occurs in SC at 17:00 on June 13, 2015. Convective overshooting is observed in a total of 8
204 pixels for C3 and their mean rain rate are over 2046.3
205 mm/h (Fig. 2g) and their mean storm top height are 16.9 km between 14 and 18 km (Fig. 2h). The
206 strongest echo occurs at 60-70 km away from point A3 and the highest echo can reach to 17.2 km, about
207 0.5 km higher than the tropopause height (Fig. 2i).

208 To learn about the characteristics of the large scale circulation of for these three cases, we calculate the
209 distribution of Precipitable Water Vapor (PWV), streamlines and Vertical Velocity (VV), shown as Fig.
210 3- and locations of the three cases are shown as the black boxes in Fig. 3. In general, the areas in
211 which convective overshooting occurs have abundant PWV and strong ascending movement. In C1,
212 PWV is between 20 and 65 mm. The PWV of the area where the precipitation case occurs (big black box)
213 is between 40 and 55 mm. The PWV of the region in which convective overshooting occurs is between
214 50 and 55 mm, which is obviously higher than else otherwise (Fig. 3a). region, which is between 50 and
215 55 mm (Fig. 3a). The vertical u Upward motion movement near the convective overshooting is strong,
216 range from between -0.03 to and -0.12 Pa/s, contributing to the occurrence of convective overshooting
217 (Fig. 3b). In C2, The PWV of C2 is more abundant than C1, and the area where the precipitation case
218 occurs is between 50 and 65 mm. The PWV of the area in which convective overshooting occurs are
219 between 50-55 and 55-60 mm (Fig. 3c). The VV near the convective overshooting is mostly between
220 -0.09 and -0.15 Pa/s (Fig. 3d). In C3, the PWV near the precipitation area and convective overshooting
221 area are the most abundant compared with C1 and C2, whose maximum can exceed 70 mm, both
222 between 65 and 75 mm (Fig. 3e), which are relatively high. The vertical u Upward movement near the
223 precipitation area and convective overshooting area are very strong and the VV are between -0.12 and
224 -0.18 Pa/s, which provide abundant water vapor and dynamic conditions for the occurrence of
225 convective overshooting.

带格式的: 字体: (中文) Times
New Roman, 10 磅, 英语(英国)

带格式的: 字体: (中文) Times
New Roman

带格式的: 字体: (中文) Times
New Roman

带格式的: 字体: (中文) Times
New Roman

带格式的: 字体: (中文) +中文正
文(宋体), (中文) 中文(中国)

226 3.2 Statistical results

227 3.2.1 Geographical distribution

228 Firstly, the horizontal distribution characteristics of convective overshooting over East China are
229 analysed by designing a more accurate algorithm for convective overshooting determination. Accurate
230 determination of tropopause height is the first step of the convective overshooting determination
231 algorithm. We first analyze geographical distribution of climatological mean of the tropopause
232 height~~tropopause~~ over East China calculated from ERA5, shown as Fig. 1b. In general, the tropopause
233 height over East China is between 11.6 km and 16.7 km and has an obvious zonal distribution pattern:
234 Tropopause height over SC and southern MEC (18-36 °N) is the highest and has small spatial variabilities,
235 concentrated at ~16.7 km. Over northern MEC (36-38 °N), tropopause height ~~obviously~~ decreases and
236 forms a gradient, which decreases to 16 km. Tropopause height over NC is the lowest~~smallest~~ and
237 continues to decrease in a gradient pattern from south to north, decreasing to 13 km near central NC
238 (45 °N) and 12 km near northern NC (48 °N). Minimum standard deviation of tropopause height appears
239 in SC, along with central and southern MEC, lower than 0.2 km. From northern MEC to northern NC, the
240 standard deviation first increases and then decreases, reaching a maximum of more than 2 km around
241 42 °N, and standard deviation over NC is generally above 1 km.

242 Obtaining storm top height from precipitation data is the second step of convective overshooting
243 algorithm. Fig. 4 show geographical distribution of storm top height for total precipitation, convective
244 precipitation and convective overshooting. Total precipitation represent the all pixels with rain rate
245 higher than 0 mm/h detected by GPM DPR, and those pixels whose rain type are “Convective” are
246 defined as convective precipitation. As shown, mean storm top height over East China ~~vary~~-varies from
247 4.5 km to 8.5 km, while convective storm top height is mainly distributed between 3.5 km and 9 km.
248 Convective storm top height over NC and northern MEC are the highest, with most areas exceeding 6.5
249 km and as we noted above, tropopause height in these two regions are lower (Fig. 1b), it can be inferred
250 that convective overshooting events are more likely to occur. Further analysis of the frequency of
251 convective overshooting in the following text will confirm this point. Compared with NC, convective
252 storm top height over SC and southern MEC is lower, mainly distributed below 6.5 km. Storm top height
253 of convective overshooting ranges from 10 km to 21 km (Fig. 4c), ~~obviously~~ much higher than normal
254 precipitation (total and convective precipitation) and increasing gradually from north to south. Storm top

255 heights of convective overshooting over NC and northern MEC are low, distributed between 10 km and
256 16 km, which is ~~due to a because that their~~ lower tropopause height (Fig. 1b) allow~~ing~~ convection with
257 lower storm top height to ~~reach the stratospherepenetrate tropo,sphere This lowers, lowering~~ the mean
258 storm top height of convective overshooting ~~in these regions~~, while ~~tropopause heights that~~ over SC and
259 southern MEC range from 16 km to 21 km (~~Fig. 1b~~), ~~with higher tropopause height (Fig. 1b)~~, allowing
260 only stronger convection to ~~reach the stratospherepenetrate the troposphere~~.
261 ~~Based on the tropopause and storm top height information calculated above, algorithm for convective~~
262 ~~overshooting determination over East China is designed and its geographical distribution of sample size~~
263 ~~and frequency are shown as Table 1 and Fig. 5~~. The frequency of convective overshooting is defined as
264 the number of convective overshooting events divided by the total observed sample number of GPM
265 DPR. Statistical results indicate that the frequency of the convective overshooting over East China is
266 very low, with a magnitude of only 10^{-3} , ~~varying regionally (Fig. 5)~~. ~~Sample size of convective~~
267 ~~overshooting over NC is the highest, followed by MEC, and SC is the lowest (Table 1)~~, ~~with regionally~~
268 ~~different. NC has the highest frequency of convective overshooting, with sample size of 2394 (count, et),~~
269 ~~followed by MEC with 582 et, and SC is the lowest (296 et)~~. Convective overshooting over NC and
270 northern MEC, whose frequency range from 4×10^{-4} to 5.4×10^{-3} (~~Fig. 5~~), occur more frequently than SC
271 and southern MEC, whose frequency is between 2×10^{-4} and 6×10^{-4} , which is mainly because the former
272 has a lower tropopause height and it's easier for convective overshooting to occur.

273 3.2.2 Vertical structures

274 Based on the reflectivity profiles and the rain-rate profiles provided by the GPM DPR instrument, we
275 studied the vertical structure of precipitation within convective overshooting. ~~Contoured Frequency by~~
276 ~~Altitude Diagrams DPDH (CFADsDistribution of Probability Density with Height)~~ analysis of radar
277 reflectivity can effectively indicate the three-dimensional structure characteristics of precipitation, which
278 is therefore applied in a large number of precipitation studies (Yuter and Houze, 1995). Fig. 6 shows
279 ~~CFADsDPDH~~ of the DPR radar reflectivity. In general, radar reflectivity within convective overshooting
280 is ~~obviously~~ stronger and its storm top height is higher. And the ~~DPDHCFADs~~ analysis also shows
281 ~~obviously~~ regional differences. Radar echo intensity of convective overshooting over NC is the weakest,
282 and the echo near surface is mainly distributed from 25 dBZ to 55 dBZ, with sharp peak ~~near~~ 47 dBZ,
283 while the peak of the total precipitation is around 16 dBZ. And the max radar echo top within convective

284 overshooting over NC can reach to 13.5 km, 3.3 km higher than the mean precipitation. Compared with
285 NC, radar reflectivity within convective overshooting over SC and MEC are stronger and their
286 ~~DPDHC~~~~FADs character is feature are~~ more similar. Their echo top height is ~18 km, 6.5 km higher than
287 total precipitation, 4.5 km higher than NC, and their echo near surface concentrated around 30-55 dBZ,
288 while that of total precipitation is between 15 dBZ and 43 dBZ. Besides, Radar reflectivity of convective
289 overshooting over NC accounts for a higher proportion below the ~~zero-freezing~~ level (~~Altitude where the~~
290 ~~temperature is 0 °C.~~), while MEC and SC account for a higher proportion above the ~~zerofreezing~~ level,
291 which indicate that the upward motion within convective overshooting over MEC and SC are stronger
292 and there are ~~larger~~~~more ice crystal particles.~~

293 Quantitative analysis of the vertical structure of precipitation within convective overshooting is one of
294 the main issues of interest to this study. Shown as Fig. 7, the rain rate profiles of convective overshooting
295 are provided, and to highlight its unique feature, rain rate profiles of total precipitation and convective
296 precipitation are also given. In general, the rain rate of convective overshooting is ~~very-much~~ higher,
297 especially below the ~~zero-freezing~~ level (~5 km), 5-10 times ~~than that of~~ normal precipitation. ~~This~~
298 ~~indicates~~~~indicating~~ stronger convection and a greater ~~concentration~~~~precipitation~~ of ice. In addition,
299 differences between three regions are obvious. Rain rate of convective overshooting over NC ~~are is~~ about
300 ~~half as high as over~~~~twice lower than~~ MEC and SC, which is consistent with the results of radar echo. At 1
301 km altitude, rain rate of convective overshooting are 12 mm/h (NC) ~~—~~, 22.5 mm/h (MEC), and 23 mm/h
302 (SC) respectively. Below ~~zerofreezing~~ level, the variation of rain rate with altitude is not very obvious,
303 and difference of rain rate between convective overshooting and normal precipitation are ~8 mm over
304 NC and ~20 mm over MEC and SC. Above ~~zerofreezing~~ level, rain rate of convective overshooting
305 ~~clearly~~ decreases ~~obviously~~ with ~~altitude~~-increasing ~~altitude~~, and rain rates are 6mm/h (NC), 10 mm
306 (MEC) and 6.5mm (SC) at 10 km. However, rain rates of other precipitation are no more than 2 mm/h
307 above 8 km, we therefore suggest that the strong upward flow within convective overshooting brings
308 large amounts of moisture from the lower layer to the upper layer.

309 We conduct the Probability Density Function (PDF) analysis on the Near Surface Rain Rate (NSRR)
310 within convective overshooting, and that of total and convective precipitation are also calculated, shown
311 as Fig. 8. Grade of precipitation are as follows: Light rain: <4.9 mm/12 h, Moderate rain: 5.0-14.9
312 mm/12h, Heavy rain: 15.0-29.9 mm/12h, Torrential rain: 30.0-69.9 mm/12h, Downpour: 70.0-139.9
313 mm/12h, and Heavy downpour: ≥140.0 mm/12h (General Administration of Quality Supervision, 2012).

314 | The PDF curve of NSRR of convective overshooting is ~~obviously~~ clearly different from normal
315 | precipitation, and has regional differences. The peak value of PDF of convective overshooting appears at
316 | ~10 mm/h, ~~belonging to~~ classified as downpour, ~~however,~~ while that of normal precipitation appears at
317 | ~1 mm/h, ~~classified as belonging to~~ moderate rain, which is obviously lower than convective
318 | overshooting. And the PDF of peak value of convective overshooting over NC is about 11.5%, while that
319 | over MEC and SC are about 6%. Besides, sample size of convective overshooting with precipitation
320 | grade of heavy downpour account for 34.0% (NC), 46.7% (MEC) and 34.8% (SC) respectively, 3-10
321 | times than normal precipitation, which remind us to pay special attention to the extreme precipitation
322 | events caused by convective overshooting that may cause harm to our production and life.

323 | 3.2.3 Microphysical features

324 | GPM center provides particle spectrum from dual-frequency radar. Based on the DSD profiles from
325 | 2ADPR, we further investigate the microphysical structures of convective overshooting. The Liquid
326 | Water Path (LWP) and Ice Water Path (IWP) show the overall water content in the atmospheric column,
327 | which is closely associated with microphysical processes within convective overshooting. To quantify
328 | the characteristics of LWP and IWP within convective overshooting, the PDF of LWP and IWP of
329 | convective overshooting are shown as Fig. 9, and that of convective and total precipitation are also
330 | shown for comparison. The LWP and IWP within convective overshooting are the highest, with high
331 | value of PDF mainly distributed around 1000 g/m^3 and 5000 g/m^3 respectively, much higher than that of
332 | normal precipitation, which are around 100 g/m^3 and 300 g/m^3 , indicating sufficient water vapor inside
333 | convective overshooting. And differences of IWP between convective overshooting and normal
334 | precipitation are bigger than LWP, suggesting that differences of water vapor above ~~zero~~freezing level
335 | between them is greater and convective overshooting brings water vapor from bottom of the troposphere
336 | to higher layers. Besides, differences of LWP and IWP between three regions are also worth noting: The
337 | LWP and IWP over MEC and SC are more similar and higher than NC. Especially, LWP over MEC has
338 | a bimodal structure with peaks of 630 and 5000 g/m^3 , which are consistent with the bimodal structure of
339 | NSRR PDF curve in Fig. 8. Analysis above in Fig. 1b shows that tropopause height over northern MEC
340 | is lower than southern MEC, making it easier for convective overshooting to occur easier happen over
341 | northern MEC. ~~This, which~~ indicates that there are two types of convective overshooting events over

342 MEC, weak events with lower storm top height and strong events with higher storm top height, which
343 correspond to the two peaks of LWP PDF curve respectively.

344 We further use DSD parameter profiles, including the effective radius (D_0) and droplet concentration
345 (dBN_0) profiles, to analyze the microphysical characteristics within convective overshooting, shown as
346 Fig. 10. Results show that the microphysical processes within convective overshooting are unique,
347 leading to various properties of the droplets in precipitation. Droplets of convective overshooting are
348 large, but sparse. Influenced by strong updrafts, precipitation particles within convective overshooting
349 continuously collide and grow large enough to fall, therefore, the effective radius of droplets are big,
350 below 10 km altitude, almost exceeding 2.5 mm, which is about twice than that of normal precipitation.
351 However, the droplet concentration within convective overshooting is relatively lower. Differences of
352 microphysical structure between three regions are also worth noting. Convective overshooting events
353 over NC have large, but sparse droplets, while that over SC have small, but dense droplets, and the
354 effective radius and concentration of droplets over MEC are between NC and SC, which is speculated
355 that it's related to the differences of aerosol content and types over three regions. Specifically, at 1 km
356 altitude, the effective radius of droplets over NC is the largest (2.87 mm), followed by MEC (2.7 mm),
357 and SC is the lowest (2.5 mm). As altitude increases, the effective radius of droplets first increase and
358 then decrease, with maximum of 2.93 mm over NC at 2.5 km and sharp peak over MEC (2.85 mm) and
359 SC (2.76 mm) near ~~zero~~freezing level, about twice than normal precipitation. The effective radius of
360 droplets for convective overshooting over NC and MEC are lower than 2.5 mm above 10 km and 12 km
361 respectively. It's worth noting that the effective radius of droplets for convective overshooting over SC
362 show an increasing trend above 8 km altitude, which are similar to convective precipitation, and their
363 effective radius of droplets over three regions also show an increasing tend from 9 km to 13 km, which
364 may be related to the strong upward motion inside. When the upward motion is strong, ice particles must
365 grow large enough to fall (Langmuir, 1948). Droplet concentration basically decreases with altitude, and
366 that within convective overshooting is obviously lower than normal precipitation and NC is the lowest,
367 while MEC and SC are higher and similar. Droplet concentration within convective overshooting near
368 ground is the highest, with NC (25.4), MEC (28) and SC (28), while that of normal precipitation is
369 mainly distributed between 32 and 35.

370 ~~Convective overshooting plays an important role in exchanging constituents and energy between~~
371 ~~troposphere and stratosphere. To quantify its impact, temperature, humidity, vertical velocity, and ozone~~

372 profiles from ERA5 are used to further analyze the internal thermodynamic characteristics of convective
373 overshooting and their impacts on atmospheric composition. The atmospheric temperature (Fig. 11aci)
374 and absolute humidity profiles within convective overshooting are statistically analyzed (Fig. 11bfj), and
375 the difference profiles between them with the total atmospheric profiles are shown as Fig.12ab. The
376 atmospheric temperature has a wavy response to convective overshooting, and the response varies in
377 different regions. Warming and cooling effect caused by convective overshooting over NC is the most
378 obvious compared with MEC and SC, no more than 1K. Near surface, convective overshooting exhibits
379 warming effect, that over NC is 2 K, and that over MEC and SC are no more than 1 K. From surface to ~2
380 km altitude, warming effect caused by convective overshooting over three regions gradually decreased.
381 From 5 km to the middle tropopause height, convective overshooting shows cooling effect over NC, with
382 sharp peak 4 K at 11.5 km altitude. Near tropopause, convective overshooting show warming effect over
383 NC and MEC, and the most warming effect over NC can reach 4 K at 16.5 km altitude; Convective
384 overshooting has an obvious humidifying effect on the air below the cloud top, with humidifying MEC
385 most and NC least. The humidification effect caused by convective overshooting first increases and then
386 decreases, with maximum of 2.3 g/m^3 (MEC), 1.45 g/m^3 (SC) and 0.8 g/m^3 (NC) at 1 km altitude.
387 To further explore dynamic structure characteristics within convective overshooting and its effect on
388 ozone, we calculated the vertical velocity profiles (Fig. 11egk) and ozone profiles (Fig. 11dhl) within
389 convective overshooting. And the difference profiles between them with the total atmospheric profiles
390 are shown as Fig.12ed. Results show that upward motion within convective overshooting is very strong,
391 the upward motion over MEC is the strongest, followed by SC and NC, and that over SC is slightly
392 higher than NC. From surface to middle tropopause, the upward motion within convective overshooting
393 firstly becomes stronger and then weakens. The vertical velocity over MEC can reach a maximum of
394 -0.85 Pa/s at 6 km altitude. The vertical velocity over SC is about -0.35 Pa/s from 6 km to 11.5 km. The
395 highest vertical velocity over NC is -0.3 Pa/s at 6.5 km. At the bottom of the stratosphere, there is a slight
396 downward movement of air, which is because the mixture of strong divergent flow and turbulence
397 mechanically drags the air above the clouds outward, and the air above the clouds are pulled down due to
398 continuity.
399 The impact of convective overshooting on ozone can be divided into three parts: Below 10 km (middle
400 and lower troposphere), convective overshooting makes ozone mass mixing ratio slightly decrease, with
401 decrease no more than $0.03 \times 10^{-6} \text{ kg/kg}$; From 10 km to 26 km (upper and middle troposphere and lower

402 ~~stratosphere), convective overshooting obviously increases ozone mass mixing ratio. The increase of~~
403 ~~ozone mass mixing ratio caused by convective overshooting over NC is the highest, with sharp peak~~
404 ~~0.3×10^{-6} kg/kg at 19 km, followed by MEC, with sharp peak 0.25×10^{-6} kg/kg at 19 km, and SC is the~~
405 ~~lowest, with sharp peak 0.1×10^{-6} kg/kg from 21 to 25 km; Above 26 km, ozone mass mixing ratio~~
406 ~~decreases obviously caused by convective overshooting, with the maximum of 0.24×10^{-6} kg/kg. The~~
407 ~~most obvious change of ozone mass mixing ratio caused by convective overshooting is the increase of~~
408 ~~ozone at tropopause and lower stratosphere, which is partly due to the strong upward motion within~~
409 ~~convective overshooting (Fig. 12e) causing the influx of ozone from lower troposphere. On the other~~
410 ~~hand, it's due to the sinking of air with high concentration ozone in the stratosphere, and the descent~~
411 ~~vertical velocity at the bottom of the stratosphere also confirms this (Fig. 12e).~~

412 **4 Summary and conclusions**

413 The microphysical characteristics of convective overshooting are essential but poorly understood due to
414 the difficulty in accurately detecting the convective overshooting and obtaining microphysical
415 parameters during severe weather events. Based on the microphysical precipitation data from GPM DPR
416 and the meteorological data from ERA5 data, we designed a more accurate algorithm for convective
417 overshooting determination and examine the particle size, concentration, phase state and other
418 parameters of the convective overshooting over East China. The main conclusions are:

419 Firstly, the horizontal distribution characteristics of convective overshooting over East China are
420 analysed by designing a more accurate algorithm for convective overshooting determination. Statistical
421 results indicate that the frequency of the convective overshooting over East China is very low, with a
422 magnitude of only 10^{-3} , with large regional differences. Convective overshooting events occur ~~obviously~~
423 more frequently over NC and northern MEC, than SC and southern MEC, mainly because of the lower
424 tropopause height of the former and the different underlying surfaces. The mean convective overshooting
425 storm top height mostly ranges from 10 km to 21 km and has obvious regional distribution differences.
426 ~~a~~And convective overshooting storm top height over NC is 5-6 km higher than SC.

427 Based on the reflectivity profiles and the rain-rate profiles provided by the GPM DPR instrument, we
428 studied the vertical structure of precipitation within convective overshooting. The ~~DPDHCFADs~~
429 analysis of the radar reflectivity shows that radar reflectivity within convective overshooting is ~~obviously~~

430 | stronger and its storm top height is higher. And the ~~DPDHC~~FADS analysis also shows obviously
431 | regional differences. Radar reflectivity of convective overshooting over NC accounts for a higher
432 | proportion below the zero-freezing level, while MEC and SC account for a higher proportion above the
433 | ~~zero~~freezing level, which indicate that the upward motion within convective overshooting over MEC and
434 | SC are stronger and there are more ice crystal particles. Rain rate results also show that rain rate within
435 | convective overshooting is higher, 5-10 times than that of normal precipitation. Especially, sample
436 | number of strong precipitation with grade of precipitation of heavy downpour accounts for 34.0% (NC),
437 | 46.7% (MEC), and 34.8% (SC), which remind us to pay special attention to the extreme precipitation
438 | events caused by convective overshooting.

439 | GPM center provides particle spectrum from dual-frequency radar. Based on the DSD profiles from
440 | 2ADPR, we further investigated the microphysical structures of convective overshooting. Statistical
441 | results show that convective overshooting has unique microphysical characteristics compared with
442 | normal precipitation, with obvious regional differences. The LWP and IWP within convective
443 | overshooting are abundant, with high values of PDF distributed around 1000 g/m^3 and 5000 g/m^3
444 | respectively. Moreover, influenced by strong updrafts, precipitation particles within convective
445 | overshooting continuously collide and grow large enough to fall, therefore, the effective radius is big,
446 | below 10 km altitude, almost exceeding 2.5 mm, which is about twice than that of normal precipitation.
447 | However, the droplet concentration within convective overshooting is relatively lower. Differences of
448 | microphysical structure between three regions are also worth noting. The effective radius of droplet over
449 | NC is slightly bigger than MEC and SC, while the droplet concentration is lower, which is speculated
450 | that it's related to the differences of aerosol content and types over three regions.

451 | ~~Convective overshooting plays an important role in exchanging constituents and energy between~~
452 | ~~troposphere and stratosphere. To quantify its impact, temperature, humidity, vertical velocity, and ozone~~
453 | ~~profiles from ERA5 are used to further analyse the internal thermodynamic characteristics of convective~~
454 | ~~overshooting and their impacts on atmospheric composition. The atmospheric temperature has a wavy~~
455 | ~~response to convective overshooting, and the response varies in different regions. Convective~~
456 | ~~overshooting has an obvious humidifying effect on the atmosphere below the cloud top, with~~
457 | ~~humidifying MEC most and NC least. The upward motion within convective overshooting is very strong,~~
458 | ~~and the order of the ascending velocity between three regions corresponds to the order of their~~
459 | ~~humidifying effects, which also reflects that the humidifying effect of convective overshooting is related~~

460 ~~to internal dynamics, consistent with study of Chae et al. (2011). In addition, convective overshooting~~
461 ~~events not only bring ozone from lower troposphere to upper troposphere and lower stratosphere, but also~~
462 ~~sink air with high concentration ozone in the stratosphere, thereby reducing the ozone in the stratosphere~~
463 ~~and lower troposphere, and obviously increasing the ozone in the upper troposphere and lower~~
464 ~~stratosphere.~~

465 Quantitative study of the internal microphysical characteristics within convective overshooting has not
466 been documented previously. Findings of this study may have important implications for the
467 microphysical evolution associated with convective overshooting, and provide more accurate
468 precipitation microphysical parameters as the input of the model simulation. This study is the
469 continuation of the previous research (Sun et al., 2021). In the future, we will further explore the impact
470 of aerosol on the internal microphysical characteristics within convective overshooting, and more
471 microphysical parameters with higher spatiotemporal resolution are expected to provide more detailed
472 features.

473 **Data availability.** ERA5 data are taken from
474 <https://www.ecmwf.int/en/forecasts/datasets/reanalysis-datasets/era5>. GPM DPR data are archived at
475 <https://gpm.nasa.gov/data/directory>.

476 **Acknowledgements.** This work was funded by the National Natural Science Foundation of China
477 Project (Grant No. 42230612) and the fellowship of China Postdoctoral Science Foundation (Grant
478 Numbers: 2022M723011).

479 **Author contributions.** Sun N., Lu G.P., and Fu Y.F. framed up this study. All the authors discussed the
480 concepts. Sun N. conducted the data analyses. Sun N. drafted the manuscript and all authors edited the
481 manuscript.

482 **Competing interests.** The authors declare no competing interests.

483 References

484 Anderson, J. G., Wilmoth, D. M., Smith, J. B. and Sayres, D. S.: UV dosage levels in summer:
485 Increased risk of ozone loss from convectively injected water vapor, *Science*, 337, 835-839,
486 <https://doi.org/10.1126/science.1222978>, 2012.

487 Avery, M. A., Davis, S. M., Rosenlof, K. H., Ye, H. and Dessler, A. E.: Large anomalies in lower
488 stratospheric water vapour and ice during the 2015–2016 El Niño, *Nature Geoscience*, 10, 405-409,
489 <https://doi.org/10.1038/ngeo2961>, 2017.

490 Alcala, C. M. and Dessler, A. E.: Observations of deep convection in the tropics using the Tropical
491 Rainfall Measuring Mission (TRMM) precipitation radar, *Journal of Geophysical Research:*
492 *Atmospheres*, 107, 4792, <https://doi.org/10.1029/2002JD002457>, 2002.

493 Biondi, R., Randel, W. J., Ho, S. P., Neubert, T. and Syndergaard, S.: Thermal structure of intense
494 convective clouds derived from GPS radio occultations, *Atmospheric Chemistry and Physics*, 12,
495 5309-5318, <https://doi.org/10.5194/acp-12-5309-2012>, 2012.

496 Bedka, K., Murillo, E. M., Homeyer, C. R., Scarino, B. and Mersiowsky, H.: The above-anvil cirrus
497 plume: An important severe weather indicator in visible and infrared satellite imagery, *Weather and*
498 *Forecasting*, 33, 1159-1181, <https://doi.org/10.1175/WAF-D-18-0040.1>, 2018.

499 Bethan, S., Vaughan, G., and Reid, S. J.: A comparison of ozone and thermal tropopause heights and the
500 impact of tropopause definition on quantifying the ozone content of the troposphere. *Quarterly*
501 *Journal of the Royal Meteorological Society*, 122(532), 929-944,
502 <https://doi.org/10.1002/qj.49712253207>, 1996,

503 Chaboureaud, J. P., Cammas, J. P., Duron, J., Mascart, P. J., Sitnikov, N. M. and Voessing, H. J.: A
504 numerical study of tropical cross-tropopause transport by convective overshoots, *Atmospheric*
505 *Chemistry and Physics*, 7, 1731-1740, <https://doi.org/10.5194/acp-7-1731-2007>, 2007.

506 Corti, T., Luo, B. P. and De Reus, M. et al.: Unprecedented evidence for deep convection hydrating the
507 tropical stratosphere, *Geophysical Research Letters*, 35, L10810,
508 <https://doi.org/10.1029/2008GL033641>, 2008.

509 Chemel, C., Russo, M. R., Pyle, J. A., Sokhi, R. S. and Schiller, C.: Quantifying the imprint of a severe
510 hector thunderstorm during ACTIVE/SCOUT-O3 onto the water content in the upper
511 troposphere/lower stratosphere, *Monthly weather review*, 137, 2493-2514,
512 <https://doi.org/10.1175/2008MWR2666.1>, 2009.

513 Chae, J. H., Wu, D. L., Read, W. G. and Sherwood, S. C.: The role of tropical deep convective clouds on
514 temperature, water vapor, and dehydration in the tropical tropopause layer (TTL), *Atmospheric*
515 *Chemistry and Physics*, 11, 3811-3821, <https://doi.org/10.5194/acp-11-3811-2011>, 2011.

带格式的: 字体: (中文) + 中文正
文 (宋体), (中文) 中文 (中国)

516 Danielsen, E. F.: In situ evidence of rapid, vertical, irreversible transport of lower tropospheric air into
517 the lower tropical stratosphere by convective cloud turrets and by larger - scale upwelling in tropical
518 cyclones, *Journal of Geophysical Research: Atmospheres*, 98, 8665-8681,
519 <https://doi.org/10.1029/92JD02954>, 1993.

520 De Reus, M., Borrmann, S. and Bansemmer, A. et al: Evidence for ice particles in the tropical stratosphere
521 from in-situ measurements, *Atmospheric Chemistry and Physics*, 9, 6775-6792,
522 <https://doi.org/10.5194/acp-9-6775-2009>, 2009.

523 Danielsen, E. F., Hipskind, R. S. and Gaines, S. E. et al.: Three-dimensional analysis of potential
524 vorticity associated with tropopause folds and observed variations of ozone and carbon monoxide,
525 *Journal of Geophysical Research: Atmospheres*, 92(D2), 2103-2111,
526 <https://doi.org/10.1029/JD092iD02p02103>, 1987.

527 ▲

528 Fueglistaler, S., Wernli, H. and Peter, T.: Tropical troposphere - to - stratosphere transport inferred from
529 trajectory calculations, *Journal of Geophysical Research: Atmospheres*, 109, D03108,
530 <https://doi.org/10.1029/2003JD004069>, 2004.

531 Frey, W., Schofield, R. and Hoor, P. et al.: The impact of overshooting deep convection on local
532 transport and mixing in the tropical upper troposphere/lower stratosphere (UTLS), *Atmospheric*
533 *Chemistry and Physics*, 15, 6467-6486, <https://doi.org/10.5194/acp-15-6467-2015>, 2015.

534 General Administration of Quality Supervision, Inspection and Quarantine of the People's Republic of
535 China: Standardization Administration of the People's Republic of China, GB/T 28592—2012 Grade
536 of precipitation, Standards Press of China, 2012.

537 Grosvenor, D. P., Choularton, T. W., Coe, H. and Held, G.: A study of the effect of overshooting deep
538 convection on the water content of the TTL and lower stratosphere from Cloud Resolving Model
539 simulations, *Atmospheric Chemistry and Physics*, 7, 4977-5002,
540 <https://doi.org/10.5194/acp-7-4977-2007>.

541 Gettelman, A., Salby, M. L. and Sassi, F.: Distribution and influence of convection in the tropical
542 tropopause region, *Journal of Geophysical Research: Atmospheres*, 107, 4080,
543 <https://doi.org/10.1029/2001JD001048>, 2002.

带格式的: 字体: (中文) +中文正
文 (宋体), (中文) 中文(中国)

544 Homeyer, C. R. and Kumjian, M. R.: Microphysical characteristics of overshooting convection from
545 polarimetric radar observations, *Journal of the Atmospheric Sciences*, 72, 870-891,
546 <https://doi.org/10.1175/JAS-D-13-0388.1>, 2015.

547 Hoffmann, L., Günther, G. and Li, D. et al.: From ERA-Interim to ERA5: the considerable impact of
548 ECMWF's next-generation reanalysis on Lagrangian transport simulations, *Atmospheric Chemistry
549 and Physics*, 19, 3097-3124, <https://doi.org/10.5194/acp-19-3097-2019>, 2019.

550 Highwood, E. J. and Hoskins, B. J.: The tropical tropopause, *Quarterly Journal of the Royal
551 Meteorological Society*, 124, 1579-1604, <https://doi.org/10.1002/qj.49712454911>, 1998.

552 [Holton, J. R., Haynes, P. H. and McIntyre, M. E. et al.: Stratosphere-troposphere exchange. *Reviews of
553 geophysics*, 33\(4\), 403-439, <https://doi.org/10.1029/95RG02097>, 1995.](#)

554 Jensen, E. J., Ackerman, A. S. and Smith, J. A.: Can overshooting convection dehydrate the tropical
555 tropopause layer?, *Journal of Geophysical Research: Atmospheres*, 112, D11209,
556 <https://doi.org/10.1029/2006JD007943>, 2007.

557 Johnston, B. R., Xie, F. and Liu, C.: The effects of deep convection on regional temperature structure in
558 the tropical upper troposphere and lower stratosphere, *Journal of Geophysical Research:
559 Atmospheres*, 123, 1585-1603, <https://doi.org/10.1002/2017JD027120>, 2018.

560 Khaykin, S., Pommereau, J. P. and Korshunov, L. et al.: Hydration of the lower stratosphere by ice
561 crystal geysers over land convective systems, *Atmospheric Chemistry and Physics*, 9, 2275-2287,
562 <https://doi.org/10.5194/acp-9-2275-2009>, 2009.

563 Langmuir, I.: The production of rain by a chain reaction in cumulus clouds at temperatures above
564 freezing, *Journal of the Atmospheric Sciences*, 5(5), 175-192,
565 [https://doi.org/10.1175/1520-0469\(1948\)005<0175:TPORBA>2.0.CO;2](https://doi.org/10.1175/1520-0469(1948)005<0175:TPORBA>2.0.CO;2), 1948.

566 Liu, N. and Liu, C.: Global distribution of deep convection reaching tropopause in 1 year GPM
567 observations, *Journal of Geophysical Research: Atmospheres*, 121, 3824-3842,
568 <https://doi.org/10.1002/2015JD024430>, 2016.

569 Liu, N., Liu, C. and Hayden, L.: Climatology and detection of overshooting convection from 4 years of
570 GPM precipitation radar and passive microwave observations, *Journal of Geophysical Research:
571 Atmospheres*, 125, e2019JD032003, <https://doi.org/10.1029/2019JD032003>, 2020.

572 Liu, C. and Zipser, E. J.: Global distribution of convection penetrating the tropical tropopause, *Journal of
573 Geophysical Research: Atmospheres*, 110, D23104, <https://doi.org/10.1029/2005JD006063>, 2005.

带格式的: 字体: (中文) +中文正
文(宋体), (中文) 中文(中国)

574 Liu, P., Wang, Y., Feng, S., Li, C. Y. and Fu, Y. F.: Climatological characteristics of overshooting
575 convective precipitation in summer and winter over the tropical and subtropical regions, *Chin. J.*
576 *Atmos. Sci.*, 36, 579-589, <https://doi.org/10.3878/j.issn.1006-9895.2011.11109>, 2012.

577 Line, W. E., Schmit, T. J., Lindsey, D. T. and Goodman, S. J.: Use of geostationary super rapid scan
578 satellite imagery by the Storm Prediction Center, *Weather and Forecasting*, 31, 483-494,
579 <https://doi.org/10.1175/WAF-D-15-0135.1>, 2016.

580 Machado, L. A. T., Rossow, W. B., Guedes, R. L. and Walker, A. W.: Life cycle variations of mesoscale
581 convective systems over the Americas, *Monthly Weather Review*, 126, 1630-1654,
582 [https://doi.org/10.1175/1520-0493\(1998\)126<1630:LCVOMC>2.0.CO;2](https://doi.org/10.1175/1520-0493(1998)126<1630:LCVOMC>2.0.CO;2), 1998.

583 Muhsin, M., Sunilkumar, S. V., Ratnam, M. V., Parameswaran, K., Murthy, B. K. and Emmanuel, M.:
584 Effect of convection on the thermal structure of the troposphere and lower stratosphere including the
585 tropical tropopause layer in the South Asian monsoon region, *Journal of Atmospheric and*
586 *Solar-Terrestrial Physics*, 169, 52-65, <https://doi.org/10.1016/j.jastp.2018.01.016>, 2018.

587 Marion, G. R., Trapp, R. J. and Nesbitt, S. W.: Using overshooting top area to discriminate potential for
588 large, intense tornadoes, *Geophysical Research Letters*, 46, 12520-12526,
589 <https://doi.org/10.1029/2019GL084099>, 2019.

590 Rodriguez - Franco, J. J. and Cuevas, E.: Characteristics of the subtropical tropopause region based on
591 long - term highly resolved sonde records over Tenerife, *Journal of Geophysical Research:*
592 *Atmospheres*, 118, 10-754, <https://doi.org/10.1002/jgrd.50839>, 2013.

593 Rossow, W. B. and Pearl, C.: 22 - year survey of tropical convection penetrating into the lower
594 stratosphere, *Geophysical research letters*, 34, L04803, <https://doi.org/10.1029/2006GL028635>,
595 2007.

596 Solomon, S., Rosenlof, K. H. and Portmann, R. W. et al.: Contributions of stratospheric water vapor to
597 decadal changes in the rate of global warming, *Science*, 327, 1219-1223,
598 <https://doi.org/10.1126/science.1182488>, 2010.

599 Sherwood, S. C. and Dessler, A. E.: A model for transport across the tropical tropopause, *Journal of the*
600 *Atmospheric Sciences*, 58, 765-779,
601 [https://doi.org/10.1175/1520-0469\(2001\)058<0765:AMFTAT>2.0.CO;2](https://doi.org/10.1175/1520-0469(2001)058<0765:AMFTAT>2.0.CO;2), 2001.

带格式的: 字体: (中文) +中文正文 (宋体), (中文) 中文(中国)

602 [Smith, J. B., Wilmouth, D. M., and Bedka, K. M. et al.: A case study of convectively sourced water](#)
603 [vapor observed in the overworld stratosphere over the United States, Journal of Geophysical](#)
604 [Research: Atmospheres, 122\(17\), 9529-9554, https://doi.org/10.1002/2017JD026831, 2017.](#)

605 Sun, N., Fu, Y., Zhong, L., Zhao, C. and Li, R.: The Impact of Convective Overshooting on the Thermal
606 Structure over the Tibetan Plateau in Summer Based on TRMM, COSMIC, Radiosonde, and
607 Reanalysis Data, Journal of Climate, 34, 8047-8063, https://doi.org/10.1175/JCLI-D-20-0849.1,
608 2021.

609 Sun, N., Fu, Y., Zhong, L. and Li, R.: Aerosol effects on the vertical structure of precipitation in East
610 China, npj Climate and Atmospheric Science, 5, 60, https://doi.org/10.1038/s41612-022-00284-0,
611 2022a.

612 Sun, N., Zhong, L., Zhao, C., Ma, M. and Fu, Y.: Temperature, water vapor and tropopause
613 characteristics over the Tibetan Plateau in summer based on the COSMIC, ERA-5 and IGRA datasets,
614 Atmospheric Research, 266, 105955, https://doi.org/10.1016/j.atmosres.2021.105955, 2022b.

615 Sherwood, S. C., Horinouchi, T. and Zeleznik, H. A.: Convective impact on temperatures observed near
616 the tropical tropopause, Journal of Atmospheric Sciences, 60, 1847-1856,
617 https://doi.org/10.1175/1520-0469(2003)060<1847:CIOTON>2.0.CO;2, 2003.

618 Takahashi, H. and Luo, Z. J.: Characterizing tropical overshooting deep convection from joint analysis of
619 CloudSat and geostationary satellite observations, Journal of Geophysical Research: Atmospheres,
620 119, 112-121, https://doi.org/10.1002/2013JD020972, 2014.

621 [Wang, X., Huang, Y., and Qu, Z. et al.: Convectively Transported Water Vapor Plumes in the](#)
622 [Midlatitude Lower Stratosphere, Journal of Geophysical Research: Atmospheres, 128\(4\),](#)
623 [e2022JD037699, https://doi.org/10.1029/2022JD037699, 2023.](#)

624 [Werner, F., Schwartz, M. J., and Livesey, N. J. et al.: Extreme outliers in lower stratospheric water](#)
625 [vapor over North America observed by MLS: Relation to overshooting convection diagnosed from](#)
626 [colocated Aqua - MODIS data, Geophysical Research Letters, 47\(24\), e2020GL090131,](#)
627 [https://doi.org/10.1029/2020GL090131, 2020.](#)

带格式的: 字体: (中文) +中文正文 (宋体), (中文) 中文(中国)

628 World Meteorological Organization.: Meteorology—A three - dimensional science: Second session of
629 the commission for aerology, WMO Bull, 4, 134-138, 1957.

630 [Xia, J.: Research on climatic regionalization of China and characteristics of temperature, humidity and](#)
631 [wind in precipitation cloud, University of Science and Technology of China, 2015.](#)

带格式的: 英语(美国)

632 Xu, W.: Thunderstorm climatologies and their relationships to total and extreme precipitation in China,
633 Journal of Geophysical Research: Atmospheres: 125, e2020JD033152,
634 <https://doi.org/10.1029/2020JD033152>, 2020.

635 Yuter, S. E. and Houze, R. A.: Three-dimensional kinematic and microphysical evolution of Florida
636 cumulonimbus. Part II: Frequency distributions of vertical velocity, reflectivity, and differential
637 reflectivity, Monthly Weather Review, 123(7), 1941-1963,
638 [https://doi.org/10.1175/1520-0493\(1995\)123<1941:TDKAME>2.0.CO;2](https://doi.org/10.1175/1520-0493(1995)123<1941:TDKAME>2.0.CO;2), 1995.

639 Zhang, A. and Fu, Y.: Life cycle effects on the vertical structure of precipitation in East China measured
640 by Himawari-8 and GPM DPR, Monthly Weather Review, 146, 2183-2199,
641 <https://doi.org/10.1175/MWR-D-18-0085.1>, 2018.

642 [Zahn, A., Brenninkmeijer, C. A. M., and Van Velthoven, P. F. J.: Passenger aircraft project CARIBIC](#)
643 [1997–2002, Part I: the extratropical chemical tropopause, Atmospheric Chemistry and Physics](#)
644 [Discussions, 4\(1\), 1091-1117, <https://doi.org/10.5194/acpd-4-1091-2004>, 2004.](#)

645

646

647

648

649

650

651

652

653

654

655

656

657

658

659

660

661

662

663

664 **Tables**

665 **Table1.** The sample number of total precipitation, convective precipitation, and convective overshooting over NC,
666 MEC, and SC.

667

Sample number (count, ct)	NC	MEC	SC
Total Precipitation	652489	546313	319127
Convective Precipitation	111903	137674	111900
Convective Overshooting	2394	582	296

668

669

670

671

672

673

674

675

676

677

678

679

680

681

682

683

684

685

686

687

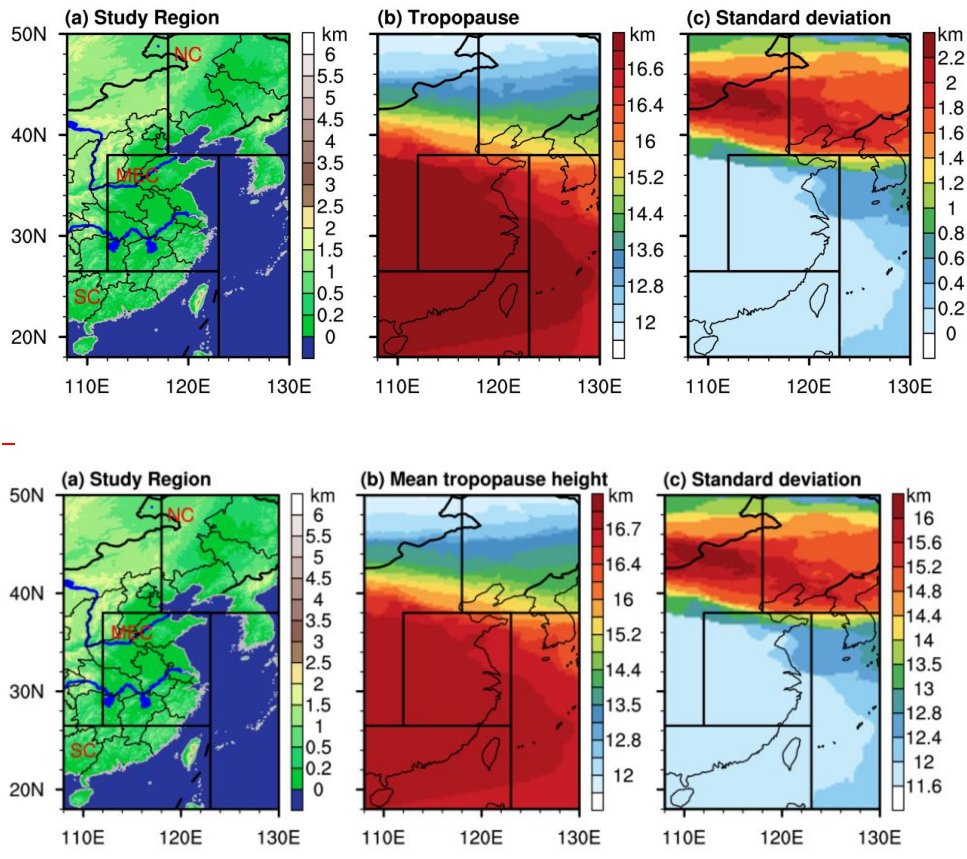
688

689

690

691
692
693
694
695
696
697
698
699
700
701
702

703 **Figures**

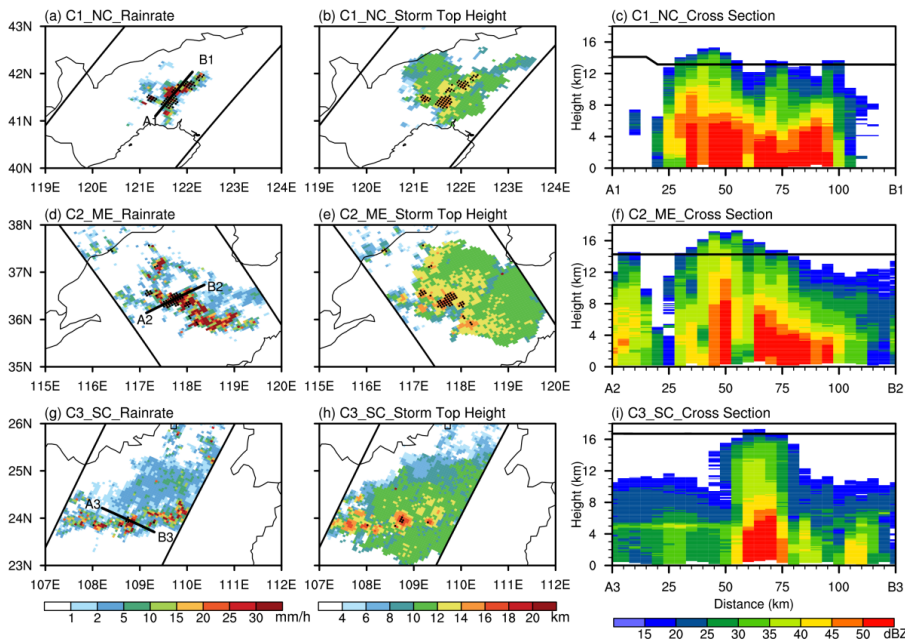


704
705

706

707 **Figure 1.** Study areas and their tropopause characteristics. (a) Regionalization of East China (Black boxes:
708 Divisions between NC, MEC and SC, and only the land surface is studied) and their terrain features. (b)
709 Distribution of Climatological mean of tropopause height from 2014 to 2020 in summer (June, July and August).
710 (c) Distribution of standard deviation of tropopause height.

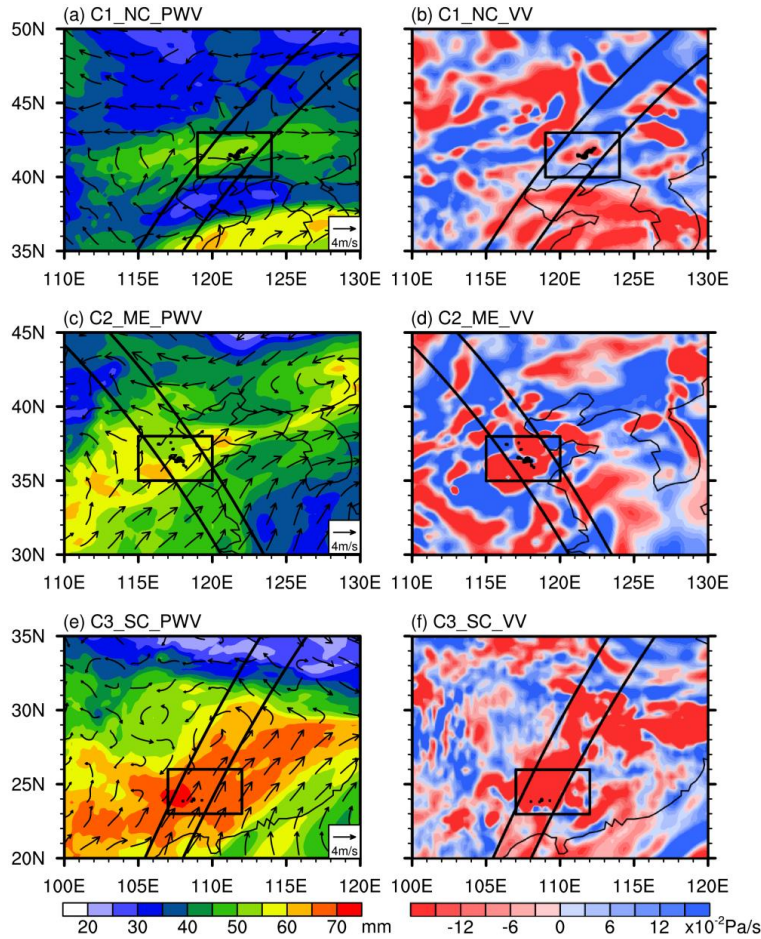
711



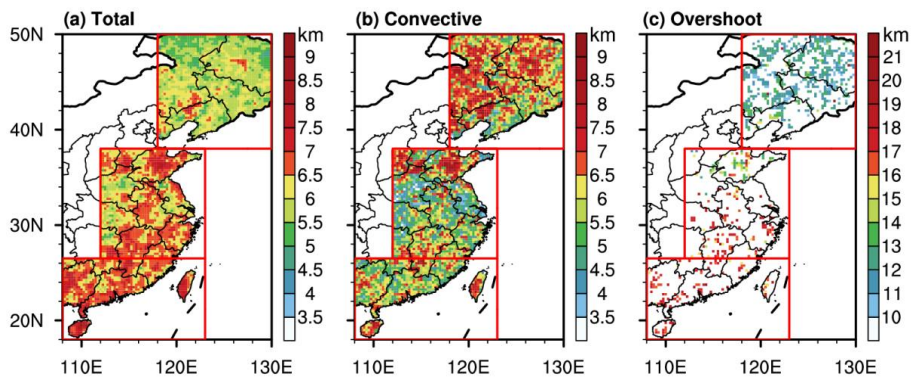
712

713 **Figure 2.** Precipitation characteristics of convective overshooting cases. (a) Distribution of rain rate of Case 1 (C1)
714 and the occurrence time of C1 is at 14:00 on July 1, 2017. (The pixels in which convective overshooting occurs are
715 marked as black boxes/points). (b) Distribution of storm top height of C1. (c) Radar reflectivity cross section along
716 A1B1 and the black line show the tropopause height along A1B1. (d) Distribution of rain rate of C2 and the
717 occurrence time of C2 is at 13:00 on July 30, 2015. (e) Distribution of storm top height of C2. (f) Radar reflectivity
718 cross section along A2B2. (g) Distribution of rain rate of C3 and the occurrence time of C3 is at 17:00 on June 13,

719 | 2015. (h) Distribution of storm top height of C3. (i) Radar reflectivity cross section along A3B3.
 720



721
 722 **Figure 3.** Characteristics of large scale circulation of convective overshooting cases. (a) Distribution of
 723 precipitable water vapor (PWV) and streamlines at 850 hPa of C1. The area where the case occurred is marked as
 724 big black boxes and the pixels in which convective overshooting occurs are marked as little black boxes. The black
 725 line is the GPM detection orbit. (b) Distribution of vertical velocity (VV) at 500 hPa of C1. (c) Distribution of
 726 PWV and streamlines of C2. (d) Distribution of VV of C2. (e) Distribution of PWV and streamlines of C3. (f)
 727 Distribution of VV of C3.
 728
 729



730

731 **Figure 4.** Geographical distribution of storm top height. (a) Distribution of storm top height for total precipitation.

732 (b) Distribution of storm top height for convective precipitation. (c) Distribution of storm top height for convective

733 overshooting.

734

735

736

737

738

739

740

741

742

743

744

745

746

747

748

749

750

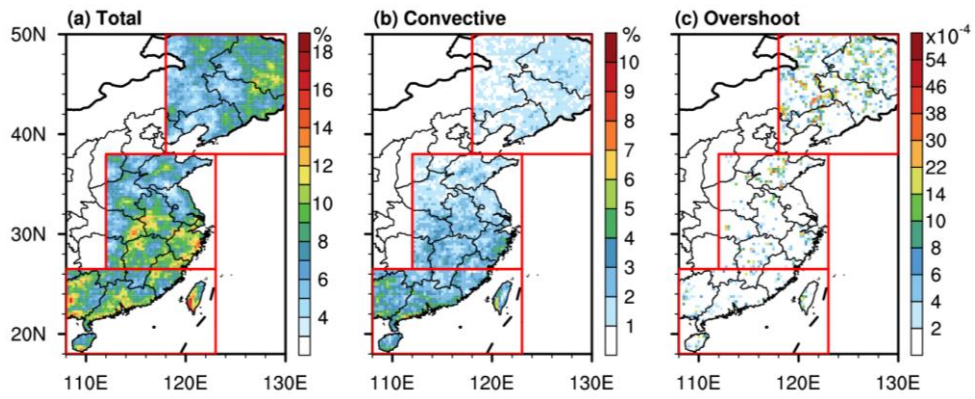
751

752

753

754

755



756

757 **Figure 5.** Precipitation frequency. **(a)** Frequency of total precipitation. **(b)** Frequency of convective precipitation.
 758 **(c)** Frequency of convective overshooting.

759

760

761

762

763

764

765

766

767

768

769

770

771

772

773

774

775

776

777

778

779

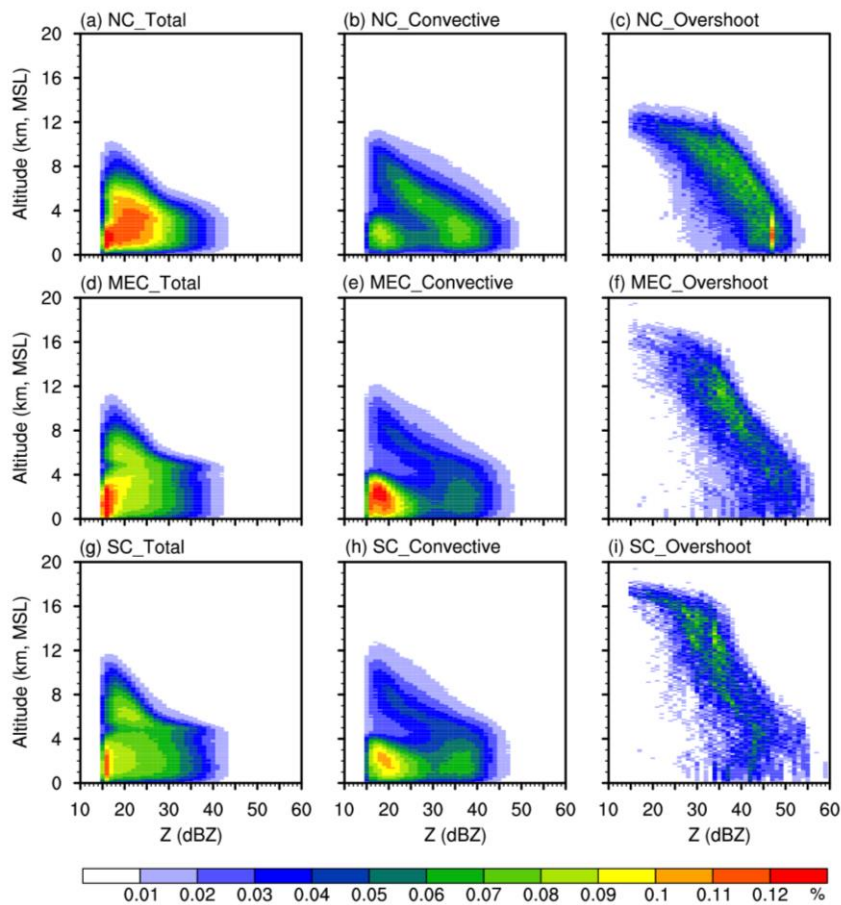
780

781

782

783

784



785

786

Figure 6. Contoured Frequency by Altitude Diagrams (CFADs) (Distribution of Probability Density with Height) of radar reflectivity. (a) CFADs for total precipitation over NC. (b) CFADs for convective precipitation over NC. (c) CFADs for convective overshooting over NC. (d) CFADs for total precipitation over MEC. (e) CFADs for convective precipitation over MEC. (f) CFADs for convective overshooting over MEC. (g) CFADs for total precipitation over SC. (h) CFADs for convective precipitation over SC. (i) CFADs for convective overshooting over SC.

792

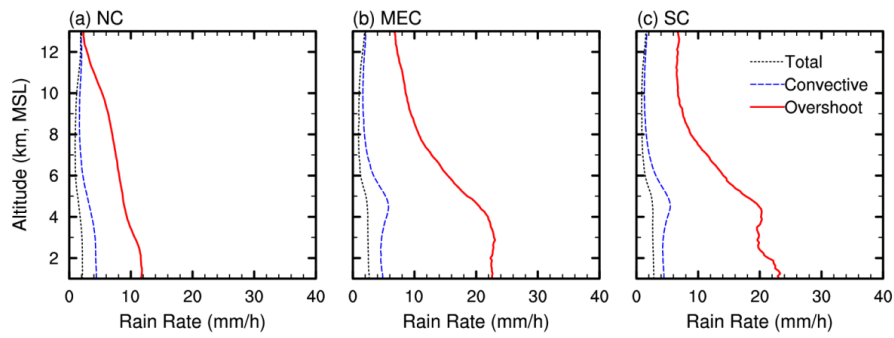
793

794

795

796

797



798

799

Figure 7. Rain rate profiles for total precipitation, convective precipitation and convective overshooting (Red lines are convective overshooting; Blue lines are the convective precipitation; Black lines are the total precipitation). **(a)** The rain rate profiles over NC. **(b)** The rain rate profiles over MEC. **(c)** The rain rate profiles over SC.

802

803

804

805

806

807

808

809

810

811

812

813

814

815

816

817

818

819

820

821

822

823

824

825

826

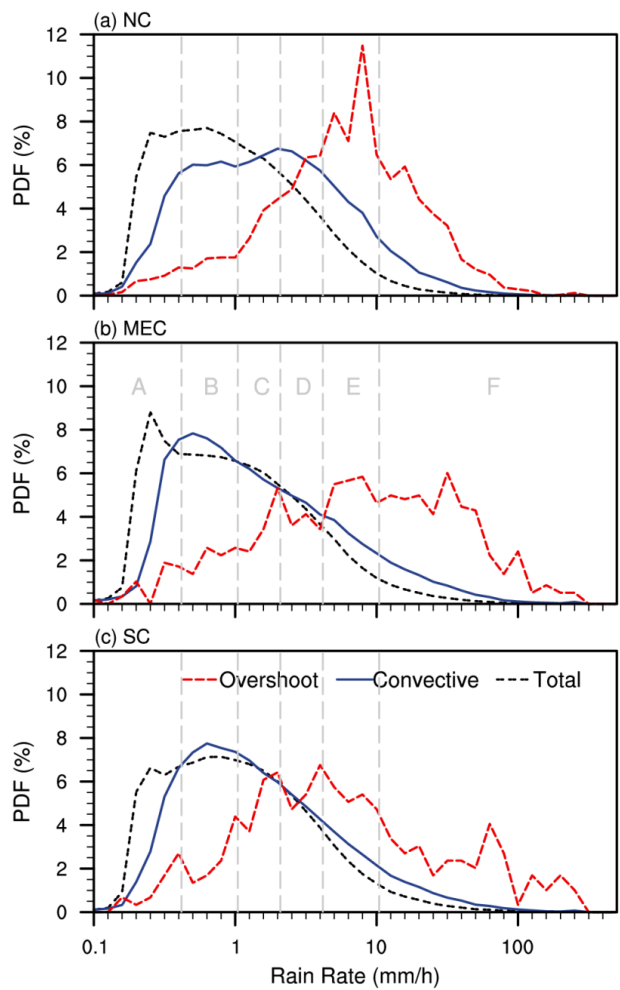
827

828

829

830

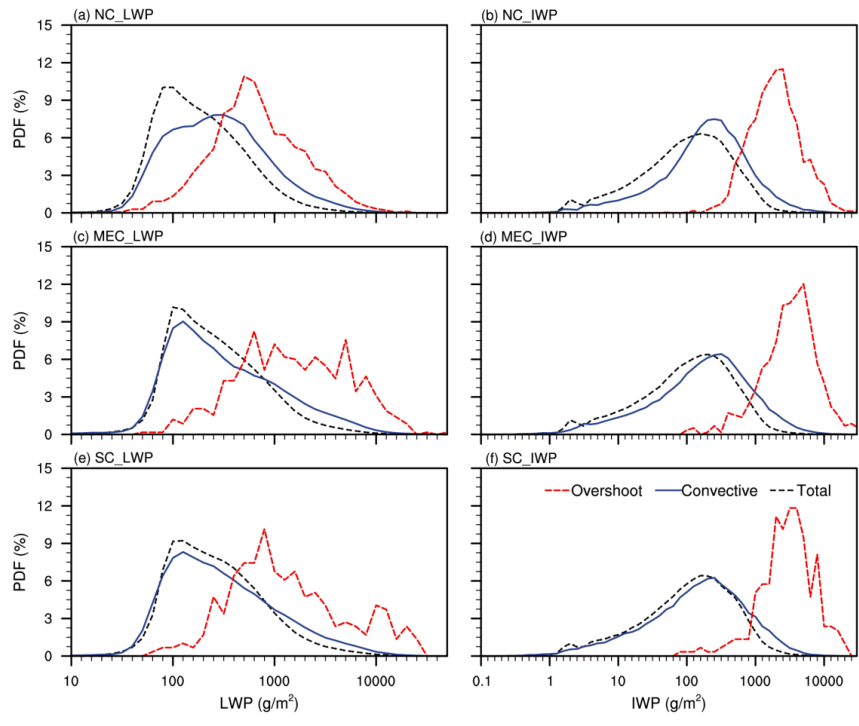
831



832

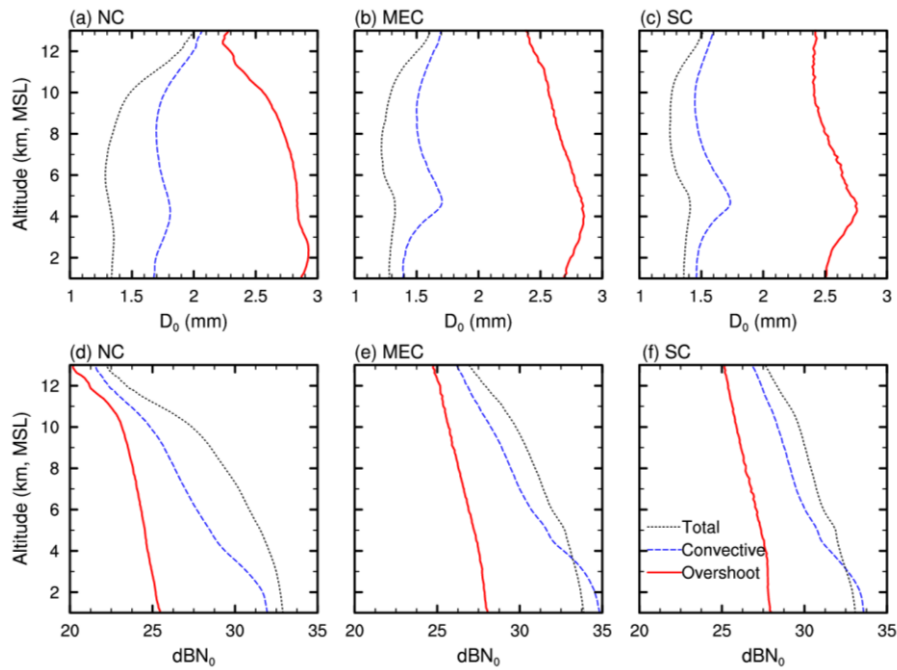
833 **Figure 8.** Probability Density Function (PDF) of Near Surface Rain Rate (NSRR). (a) PDF of NSRR in NC. (b)

834 PDF of NSRR in MEC. (c) PDF of NSRR in SC.



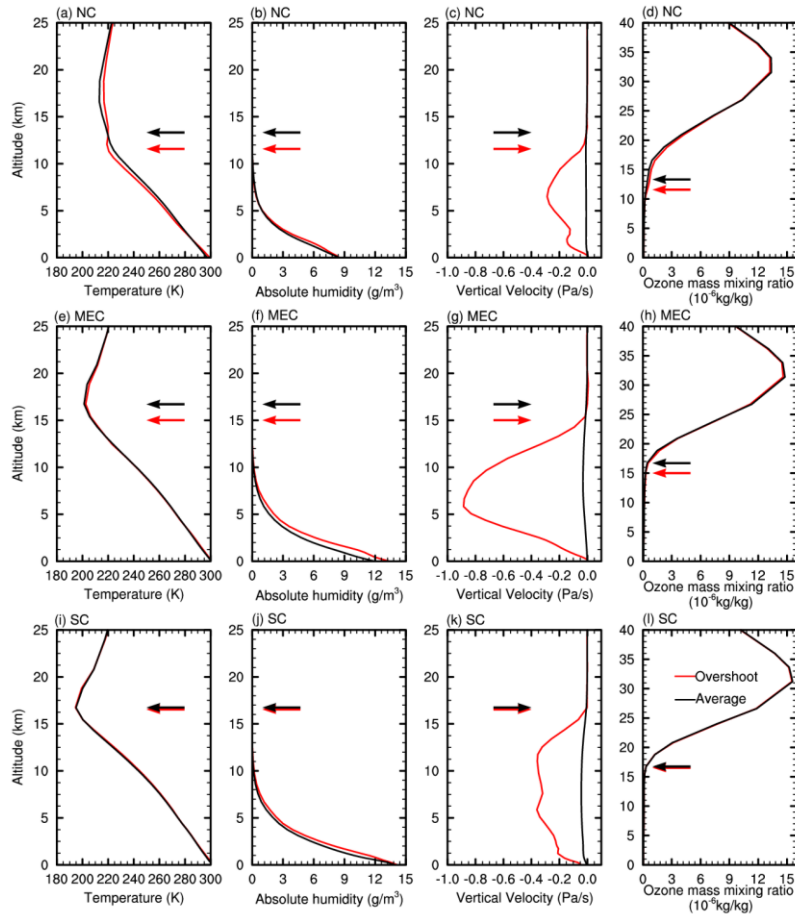
835
 836 **Figure 9.** PDF of Liquid Water Path (LWP) and Ice Water Path (IWP). **(a)** PDF of LWP over NC. **(b)** PDF of IWP
 837 over NC. **(c)** PDF of LWP over MEC. **(d)** PDF of IWP over MEC. **(e)** PDF of LWP over SC. **(f)** PDF of IWP over
 838 SC.

839
 840
 841
 842
 843
 844
 845
 846
 847
 848
 849
 850
 851
 852
 853
 854



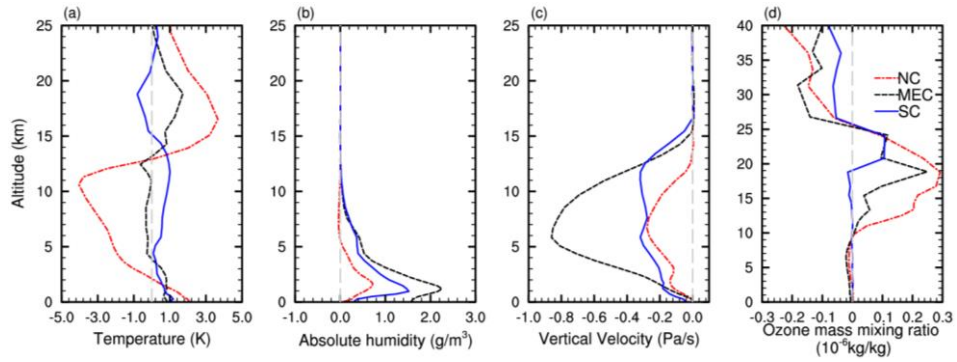
855
 856
 857
 858
 859
 860
 861
 862
 863
 864
 865
 866

Figure 10. The droplet concentration (dBN_0) and effective radius (D_0) profiles for total precipitation, convective precipitation and convective overshooting over NC, MEC and SC. **(a)** The dBN_0 profiles over NC. **(b)** The dBN_0 profiles over MEC. **(c)** The dBN_0 profiles over SC. **(d)** D_0 profiles over NC. **(e)** D_0 profiles over MEC. **(f)** D_0 profiles over SC.



867
 868
 869
 870
 871
 872
 873
 874
 875
 876

Figure 11. Atmospheric parameter profiles for total precipitation and convective overshooting over NC, MEC and SC. (a) Temperature profiles over NC. (b) Absolute humidity profiles over NC. (c) Vertical velocity profiles over NC. (d) Ozone mass mixing ratio profiles over NC. (e) Temperature profiles over MEC. (f) Absolute humidity profiles over MEC. (g) Vertical velocity profiles over MEC. (h) Ozone mass mixing ratio profiles over MEC. (i) Temperature profiles over SC. (j) Absolute humidity profiles over SC. (k) Vertical velocity profiles over SC. (l) Ozone mass mixing ratio profiles over SC.



877
 878 **Figure 12.** Difference of atmospheric parameters profiles between total precipitation and convective overshooting
 879 over NC, MEC and SC. (a) Difference of temperature profiles. (b) Difference of absolute humidity profiles. (c)
 880 Difference vertical velocity profiles.—

881
 882
 883
 884
 885
 886